THE JOURNAL OF PHYSICAL CHEMISTRY Letters

pubs.acs.org/JPCL

Unidirectional Energy Transfer in Conjugated Molecules: The Crucial Role of High-Frequency C≡C Bonds

S. Fernandez-Alberti,[†] Valeria D. Kleiman,[‡] S. Tretiak,[§] and Adrian E. Roitberg*[,⊥]

[†]Universidad Nacional de Quilmes, Roque Saenz Peña 352, B1876BXD Bernal, Argentina, [‡]Department of Chemistry and Center for Chemical Physics, University of Florida, Gainesville, Florida 32611, [§]Theoretical Division, Center for Nonlinear Studies (CNLS), and Center for Integrated Nanotechnologies (CINT), Los Alamos National Laboratory, Los Alamos, New Mexico 87545, and [⊥]Quantum Theory Project, Department of Chemistry, University of Florida, Gainesville, Florida 32611

ABSTRACT Excited-state nonadiabatic molecular dynamics is used to study energy transfer in dendrimer building blocks, between two-, three-, and four-ring linear polyphenylene ethynylene units linked by meta-substitutions. Upon excitation, dendrimers with these building blocks have been shown to undergo highly efficient and unidirectional energy transfer. The simulations start by initial vertical excitation to the S_4, localized on the two-ring unit. We observe ultrafast directional $S_4 \rightarrow S_3 \rightarrow S_2 \rightarrow S_1$ electronic energy transfer, corresponding to sequential two-ring → three-ring → four-ring transfer. The electronic energy transfer is concomitant with vibrational energy transfer through a dominant C≡C stretching motion. Upon $S_{n+1} \rightarrow S_n$ population transfer, a rapid increase of the $S_{n+1}-S_n$ energy gaps and decrease of the corresponding values for S_n-S_{n-1} gaps are observed. As a consequence, the S_{n+1} and S_n states become less coupled, while the S_n and S_{n-1} become more coupled. This behavior guarantees the successful $S_{n+1} \rightarrow S_n \rightarrow S_{n-1}$ unidirectional energy transfer associated with the efficient energy funneling in light-harvesting dendrimers.

SECTION Electron Transport, Optical and Electronic Devices, Hard Matter

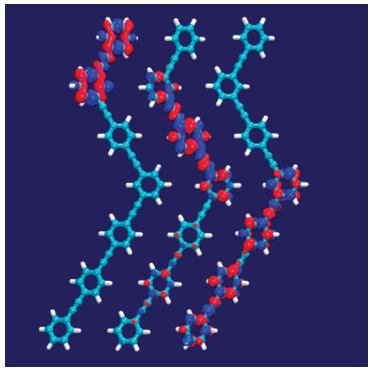

The development of new materials with applications to light-harvesting and transport for solar cells represent a major task to address the global challenge of renewable energy resources.[1−4] Advances in organic synthesis can yield macromolecules with well-defined structures,[5−7] and it has become possible to synthesize artificial light-harvesting dendritic macromolecules[8] with built-in energy gradients. Such dendrimers are branched conjugated macromolecules with regular structures, allowing very efficient energy funneling through the molecular system.

Dentritic macromolecules are arrays of coupled chromophores, with the energy of each unit depending on backbone structure and conformation (affected by nuclear dynamics).[3,6,9−12] The relative strengths of the couplings between units control the exciton transport, which competes with deactivation.[13−17] Pathways of intramolecular vibrational energy flow can be associated with the ultrafast electronic energy-transfer process.[18]

Previous results from a wide variety of symmetric and unsymmetric dendrimers has provided a qualitative picture of energy gradients,[19,20] including their relation to dendrimer size, architecture, and energy transfer. Recent experiments reported by Kleiman et al.[21] have shown that the coherent control of excited-state dynamics in dendritic macromolecules is possible.

From a theoretical point of view, the complexity of the dendritic architectures makes it difficult to explore the interplay between nuclear motion and electronic couplings that guarantees the efficient energy funneling.[22−24] Simple approaches such as the Förster framework for modeling energy-transfer rates frequently fail to reproduce experimental observables in such complex macromolecules.[15,25,26] Less complex systems, composed of model building blocks, are useful to investigate the process.[27]

In this paper, we study the ultrafast electronic and vibrational energy transfer in a building block of a well-known dendrimer (the nanostar[3]). The energy transfer occurs between two-, three-, and four-ring linear polyphenylene ethynylene (PPE) units linked through meta-substitutions, as shown in Figure 1(inset). The meta-branching localizes excitons within each linear fragment, with relatively small leakage into the next section of the molecule. We use this system as a model to understand the successful directional energy transfer that takes place in more complex phenylethynylperylene-terminated dendrimers.[12,28−30] In those systems, the light-harvesting action takes place by a highly

Received Date: June 9, 2010
Accepted Date: August 27, 2010
Published on Web Date: September 02, 2010

DOI: 10.1021/jz100794z | *J. Phys. Chem. Lett.* **2010**, *1*, 2699–2704

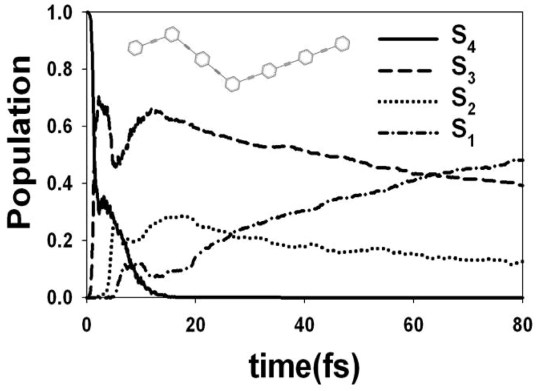

Figure 1. Population on each electronic surface as a function of time obtained from the fraction of trajectories in each state. Similar trends are observed up to 150 fs. Inset: Chemical structure of the phenylene ethynylene (PE) building block. The molecule has two-, three-, and four-ring linear PE units linked by meta-substitution.

efficient intramolecular transfer of the energy absorbed at the periphery (two-ring units, high frequency) through the dendritic branches (three-ring and four-ring units) to the perylene core.

In this work, nonadiabatic molecular dynamics simulations[31] are performed using molecular dynamics with quantum transitions (MDQT), as described by Tully,[32−34] which has been successfully applied to a large variety of photochemical reaction mechanisms in organic compounds.[18,31,35−50] This procedure has been recently implemented in the semiempirical NA-ESMD (nonadiabatic excited-state molecular dynamics) code,[51−53] where the electronic energies, gradients, and nonadiabatic coupling vectors for the excited states are calculated on-the-fly during the molecular dynamics simulations using the collective electronic oscillator (CEO) method.[54,55] The CEO code is based on well-tested semiempirical models combined with the time-dependent Hartree−Fock (TDHF) or the configuration interaction singles (CIS) formalism to describe correlated excited states. Details about the method can be found elsewhere.[54,55] The clear advantages of this method include its speed, scalability with a number of atoms, and, more importantly, efficient calculation of analytical gradients for the excited-state surfaces, permitting the use of molecular dynamics.

MDQT treats the electronic degrees of freedom quantum mechanically, while the motion of the nuclei is treated classically. In our current implementation, the electronic wave function is written as

$$\Psi(r,R,t) = \sum_{I}^{N} C_I(t)\psi_I(r;R) \qquad (1)$$

where r and R are the electronic and nuclear coordinates respectively. $N = 10$ is the number of excited states considered, with $\psi_I(r;R)$ being their eigenstates. We use a CIS level to represent excited states calculated with the CEO code using the AM1 Hamiltonian.[56] The use of this semiempirical level of theory has been validated in our previous work on a related system.[53] Furthermore, the AM1 semiempirical formalism has been validated for description of the PES in conjugated polymers, PPV[51] polyfluorenes,[57,58] and the accuracy of semiempirical approaches for excitation energies in a variety of conjugated organic molecules has been benchmarked in ref 59. The vertical excitation energies and oscillator strengths for the S1−S4 states calculated at the AM1/CIS level for an AM1-optimized structure have been compared with calculations at different levels of theory (see Supporting Information (Table I)), obtaining a qualitatively reasonable agreement between them. NA-ESMD is a numerically tractable method able to propagate a few hundred trajectories with selected initial conditions along different excited-state potential energy surfaces in large molecular systems on ps time scales.

The coefficients $C_I(t)$ evolve in time according to

$$i\hbar\dot{C}_I(t) = C_I(t)E_I - i\hbar\sum_{J} C_J(t)\dot{R}d_{IJ} \qquad (2)$$

where $d_{IJ} = \langle\psi_I(r;R)|\nabla_R\psi_J(r;R)\rangle$ is the nonadiabatic coupling vector.

Initial conditions were collected from a molecular dynamics simulation in the electronic ground state at 10 K, equilibrated over 500 ps. The initial configurations taken every ps have been chosen for excited-state dynamics simulations. In every snapshot, we obtain the excited-state structure by analyzing the spatial extent of the state transition densities (S_n−S_0); both S_1 and S_3 states are localized on the four-unit linear segment, whereas the S_2 and S_4 states are localized on the three-ring and two-ring units, respectively. These features can be seen in Figure 1 in the Supporting Information, where transition densities corresponding to $S_0 \rightarrow S_1$, S_2, and S_4 are shown. Consequently, the photoinduced energy transfer from two to four rings can occur through two distinct scenarios,[60] (a) the through-space direct process via $S_4 \rightarrow S_3$ and $S_4 \rightarrow S_1$ pathways and (b) the through-bond sequential transfer via $S_4 \rightarrow S_2 \rightarrow S_1$ mechanism. To understand this dynamics, our nonadiabatic excited-state trajectories were started after a vertical excitation to the S_4 state, which corresponds to the first optically allowed state spatially localized on the two-ring unit.

We performed 500 independent MDQT trajectories of 150 fs each using a Langevin thermostat to keep the temperature[61] constant at 10 K with a friction coefficient γ of 2.0 ps^{-1}. A true comparison of time scales with experiments needs either a correct value of the friction coefficient or the presence of real solvent molecules.[62] We are working on these two approaches, and they will be presented in future work. The velocity Verlet algorithm[63] was used with a time step of 0.05 fs for the classical nuclei. The electronic C_I coefficients (eq 2) were propagated using a gear predictor corrector algorithm[64] with a δt of 1.25×10^{-5} fs (4000 times shorter than the classical time step)

Figure 1 displays the time dependence of the average populations for the different electronic states during the MDQT trajectories. We show results only from 0 to 80 fs, but populations follow the same trends from 80 to 150 fs. The initially excited S_4 state depopulates almost immediately to the S_3 state. No hops from the S_4 state to higher states have been observed. The system remains on the same diabatic

DOI: 10.1021/jz100794z | J. Phys. Chem. Lett. 2010, 1, 2699–2704

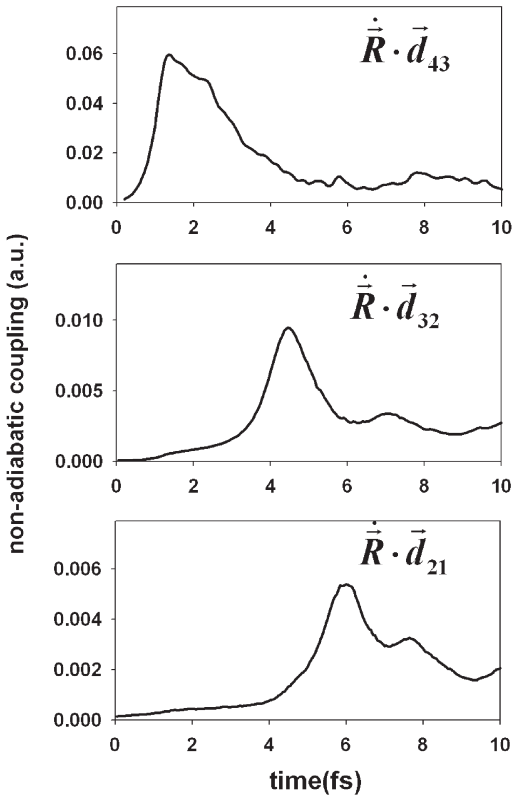

Figure 2. Time-dependent nonadiabatic couplings averaged over all trajectories.

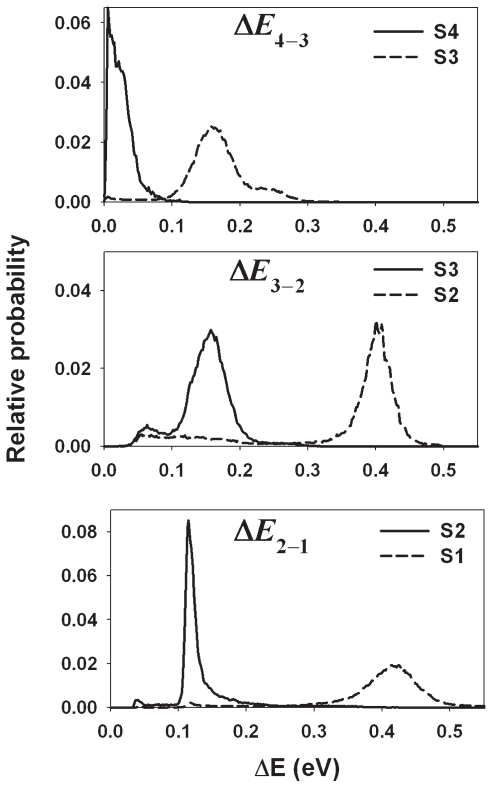

Figure 3. Histograms of the energy gap $\Delta E_{(n+1)-n}$ between the $S_{(n+1)}$ and S_n ($n = 1-3$) states. Solid lines correspond to the energy gaps while nuclei are moving on the $S_{(n+1)}$ potential energy surface, and dashed lines correspond to the gaps while the nuclei move on the S_n state.

state, which is spatially localized on a two-ring unit after the crossing point for almost all trajectories. Thus, we do not observe any significant direct through-space two-to-four ring transfer via S_4/S_3 crossing (or S_4/S_1 crossing). S_4/S_3 crossing is an example of a trivial unavoided crossing when the system remains on the same diabatic state. We further denote $S_4/S_3(2)$ and $S_4/S_3(4)$ as being the diabatic states localized on the two- and four-ring units. A S_4/S_3 recurrence pattern is observed during the first 10 fs, indicating that the system passes twice through the region of S_4/S_3 crossing. After that, a highly efficient, sequential $S_4/S_3(2) \rightarrow S_2 \rightarrow S_1$ mechanism of electronic energy transfer between the PPE units is observed, in agreement with the near-unity values of the quantum yield for energy reported for the nanostar. This unidirectional mechanism is a direct consequence of the distinct values of the nonadiabatic couplings to move to a surface below and to a surface above the present one. As shown in eq 2, the value of $\dot{R}d_{I,J}$ determines the strength of the chance of jumping from state I to state J. The time dependence of the nonadiabatic couplings $Rd_{I,J}$ averaged over all trajectories is shown in Figure 2. Large values of $\dot{R}d_{4,3}$ are seen at very early times after photoexcitation. This corresponds to the passage of trajectories through the region of the unavoided crossing between the S_4 and S_3 states. Only after the decrease of $Rd_{4,3}$, an increase of $\dot{R}d_{3,2}$ is observed, corresponding to the moment when vibrational relaxation brings the $S_4/S_3(2)$ state energy into close proximity to the S_2 state energy. The $S_4/S_3(2)$ and S_2 states are not coupled before that, and they do not remain coupled for a long time. Finally, only after the increase of $\dot{R}d_{3,2}$, an increase in the coupling $\dot{R}d_{2,1}$ takes place. Therefore, the states are sequentially coupled as pairs, and the system does not seem to undergo regions of simultaneous large nonadiabatic couplings among several excited states. After the states S_{n+1} and S_n pass through the peak of their nonadiabatic coupling, the coupling between S_n and S_{n-1} starts to increases, while the coupling between S_{n+1} and S_n decreases. This effect ensures sequential unidirectional energy transfer.

To understand the reasons leading to this behavior, we explore the role of the nuclear differential motion on the different potential energy surfaces. Figure 3 displays histograms for the energy gap $\Delta E_{(n+1)-n}$ between the $S_{(n+1)}$ and S_n ($n = 1-3$) states. The value of $\Delta E_{(n+1)-n}$ is smaller when the nuclei move on the potential energy surface of the $S_{(n+1)}$ state than that when they move on the S_n state. That is, while the nuclear motion is on the $S_{(n+1)}$ state, the $S_{(n+1)}$ and S_n states get closer in energy, but as the nuclei move on the S_n state, the energy gap increases, separating the surfaces. Since the nonadiabatic couplings $d_{(n+1)-n}$ are proportional to $1/\Delta E_{(n+1)-n}$, according to the Hellmann–Feynman theorem,[65] the nuclear motion on the $S_{(n+1)}$ surface couples the $S_{(n+1)}$ and S_n states, while the motion on the S_n surface decouples them. The difference in the nuclear dynamics in the $S_{(n+1)}$ and S_n states enhances the funneling signature of the energy-transfer mechanism.

DOI: 10.1021/jz100794z | J. Phys. Chem. Lett. 2010, 1, 2699–2704

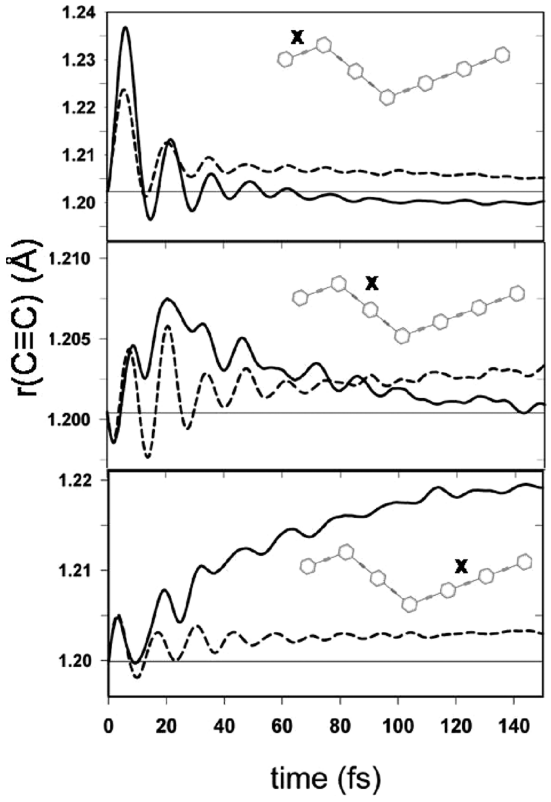

Figure 4. Length of particular ethynylene bonds (labeled X) as a function of time obtained from averaged trajectories. Solid lines correspond to trajectories that undergo electronic energy transfer all the way to the S_1 state, and dashed lines are averages over those trajectories that do not reach the S_1 state.

In MDQT trajectories, changes in the $C_I(t)$ coefficients (eq 2) induce transitions or hops between the states. These transitions result in a sudden change in forces exerted on the classical nuclei due to the change in the potential energy surface guiding the dynamics. The transition force[34] that acts to redistribute the energy of the electronic gap between the adiabatic states into the nuclear kinetic energy is in the direction of the nonadiabatic coupling vector d_{IJ}. Similar to our previous study,[53] major contribution to these vectors comes from the stretching motions in the direction of the ethynylene bonds (C≡C). More precisely, the main contribution to $d_{4,3}$ comes from the triple bond on the two-ring component (43%); the triple bonds on the two- and three-ring components contribute significantly to $d_{3,2}$ (44%), and those on the three- and four-ring components contribute mainly to $d_{2,1}$ (44%). We conclude that nuclear motions in the direction of the stretching of ethynylene bonds are related to the efficiency of the energy transfer.

To follow intramolecular vibrational energy redistribution, we monitored the ethynylene bond lengths as a function of time (Figure 4). Trajectories were divided according to their success in eventually reaching the S_1 state. Solid lines represent the C≡C bond length (labeled with an X) for trajectories that end on S_1, while the dashed lines represent the trajectories that do not end on S_1. Immediately after excitation to S_4, the triple bond length of the two-ring component experiences a sudden increase. Then, the bond undergoes an ultrafast relaxation that follows the $S_4/S_3 \rightarrow S_2$ electronic energy transfer (Figure 1). At the end of our simulations, larger values of this ethynylene bond length are obtained for trajectories that do not end on S_1 (dashed line) with respect to the ones that undergo electronic energy transfer (solid line), indicating higher levels of vibrational excitation and trapping of the electronic energy on the two-ring unit (exciton self-trapping phenomenon previously observed in conjugated polymers[66]). Accompanying the electronic energy transfer, both ethynylene bonds of the three-ring system become excited since the S_2 state is mainly localized on the three-ring unit. After that, trajectories that finish on the S_1 state do not keep the excess energy localized in the three-ring PE unit; instead, they show a rapid relaxation of the ethynylene bonds. Those trajectories that do not reach the S_1 state remain elongated, indicating that the excess vibrational energy gets trapped in the three-ring PE units. Finally, the ethynylene bonds of the four-ring system receive the excess vibrational energy. This process follows the $S_2 \rightarrow S_1$ electronic energy transfer, and it is not observed on trajectories that do not reach the S_1 state. To summarize, the ultrafast $S_4/S_3 \rightarrow S_2 \rightarrow S_1$ electronic energy transfer is followed by an also ultrafast two-ring → three-ring → four-ring vibrational energy transfer as measured by the elongation of the ethynylene bonds on the different PE units.

Finally, we analyze the way by which the electronic energy transport is modulated by nuclear dynamics. For this purpose, we follow the average values of the different ethynylene bonds during hops. While the initial value of the triple bond of the two-ring system is 1.202 Å, its value during $S_4 \rightarrow S_3$ and $S_3 \rightarrow S_2$ hops are 1.211 and 1.227 Å, respectively. This is in agreement with the initial large-amplitude motion of this bond shown in Figure 4 and the simultaneous ultrafast initial transfer of electronic population shown in Figure 1. The relaxation of this bond following the $S_4/S_3 \rightarrow S_2$ electronic energy transfer leads to a final value of 1.203 Å during the final $S_2 \rightarrow S_1$ hops. The stretching of the ethynylene bonds of the three-ring system does not present significant differences with respect to its average initial values of 1.200 Å until the $S_2 \rightarrow S_1$ hop, where they reach the average values of 1.213 Å. No significant differences are observed in the values of the triple bond lengths of the four-ring system during any process of electronic energy transfer. Within a good level of approximation, the excess energy introduced in the system during laser photoexcitation can be considered large enough (with a significant transient increase in the temperature of the molecule) to minimize the effects that the inclusion of the vibrational zero-point energy can have on the nuclear motion. Therefore, the only quantum effect that we observe is the one concerning the electronic energy transfer. The activation of the stretching modes occurs not because of the bath temperature but because optical excitation lands the system into an excited state far from equilibrium. The system becomes vibrationally excited instantaneously. Coupling to the solvent (represented here by a Langevin term) and to other intramolecular modes provides the vibrational de-excitation channels. Temperature effects allow sampling of some conformational space along the trajectory of the wavepacket due to strong Franck−Condon effects.

DOI: 10.1021/jz100794z | J. Phys. Chem. Lett. 2010, 1, 2699–2704

In summary, in this Letter, we simulate the highly efficient sequential $S_4/S_3(2) \rightarrow S_2 \rightarrow S_1$ mechanism of electronic energy transfer between phenylene ethynylene building blocks using nonadiabatic molecular dynamics simulations. The mechanism was shown to be a sequential passage of the system through regions with differential relative values of the nonadiabatic couplings. A progressive delay to reach the regions of large nonadiabatic couplings is observed. The system undergoes strong coupling between states in a sequential order, and the couplings involve only one pair of states at a time. Electronic energy transfer is concomitant to intramolecular vibrational energy redistribution, with the nuclear motions in the direction of the ethynylene bonds playing a critical role in the process.

SUPPORTING INFORMATION AVAILABLE Comparison of the vertical excitation energies and oscillator strengths for electronic excitations and transition density isosurfaces. This material is available free of charge via the Internet at http://pubs.acs.org.

AUTHOR INFORMATION

Corresponding Author:

*To whom correspondence should be addressed.

ACKNOWLEDGMENT This work was partially supported by CONICET, UNQ, NSF Grant CHE-0239120, and the Center for Integrated Nanotechnologies, a U.S. Department of Energy, Office of Basic Energy Sciences user facility. We also acknowledge support of the Center for Nonlinear Studies (CNLS) at LANL. We acknowledge UF's High-Performance Computing Center and NSF Large Allocations Resource Committee through Grants TG-MCA05S010 and UT-NTNL0002 for providing computational resources.

REFERENCES

(1) Lewis, N. S.; Nocera, D.G. Powering the planet: Chemical challenges in solar energy utilization. *Proc. Natl. Acad. Sci. U.S.A.* **2006,** *103*, 15729–15735.
(2) Benniston, A. C.; Harriman, A. Artificial Photosynthesis. *Mater. Today* **2008,** *11*, 26–34.
(3) Swallen, S. F.; et al. Dendrimer Photoantenna Supermolecules: Energetic Funnels, Exciton Hopping and Correlated Excimer Formation. *J. Mol. Struct.* **1999,** *485*, 585–597.
(4) Mobius, D.; Kuhn, H. Energy Transfer in Monolayers with Cyanine Dye Sheibe Aggregates. *J. Appl. Phys.* **1988,** *64*, 5138–5141.
(5) Lecuiller, R.; et al. Dual Resonance Fluorescence of Polydiacetylene Chains Isolated in Their Crystalline Monomer Matrix. *Phys. Rev. Lett.* **1998,** *80*, 4068–4071.
(6) Frechet, J. M. J. Functional Polymers and Dendrimers — Reactivity, Molecular Architecture, and Interfacial Energy. *Science* **1994,** *263*, 1710–1715.
(7) Jiang, D. L.; Aida, T. Photoisomerization in Dendrimers by Harvesting of Low-Energy Photons. *Nature* **1997,** *388*, 454–456.
(8) Fréchet, J. M. J.; Tomalia, D. *Dendrimers and Other Dendritic Polymers*; John Wiley and Sons: West Sussex, 2001.
(9) Mukamel, S. Photochemistry — Trees to trap photons. *Nature* **1997,** *388*, 425.
(10) Swallen, S. F.; et al. Correlated Excimer Formation and Molecular Rotational Dynamics in Phenylacetylene Dendrimers. *J. Phys. Chem. B* **2000,** *104*, 3988–3995.
(11) Rana, D.; Gangopadhyay, G. Steady-State Spectral Properties of Dendrimer Supermolecule As a Light Harvesting System. *Chem. Phys. Lett.* **2001,** *334*, 314–324.
(12) Kopelman, R.; et al. Spectroscopic Evidence for Excitonic Localization in Fractal Antenna Supermolecules. *Phys. Rev. Lett.* **1997,** *78*, 1239.
(13) Tretiak, S.; Mukamel, S. Density Matrix Analysis and Simulation of Electronic Excitations in Conjugated and Aggregated Molecules. *Chem. Rev.* **2002,** *102*, 3171–3212.
(14) Kirkwood, J. C.; et al. Simulations of Energy Funneling and Time- And Frequency-Gated Fluorescence in Dendrimers. *J. Chem. Phys.* **2001,** *114*, 2419–2429.
(15) Ortiz, W.; et al. Energy Transfer in the Nanostar: The Role of Coulombic Coupling and Dynamics. *J. Phys. Chem. B* **2005,** *109*, 11512–11519.
(16) Tortschanoff, A.; Piryatinski, A.; Mukamel, S. Femtosecond Pump—Probe Spectroscopy of the Dendrimeric Nanostar. *J. Lumin.* **2001,** *94*, 569–573.
(17) Tortschanoff, A.; Mukamel, S. Pump—Probe Simulation Study of the Two-Exciton Manifold of Dendrimers. *J. Phys. Chem. A* **2002,** *106*, 7521–7529.
(18) Prezhdo, O. V.; Duncan, W. R.; Prezhdo, V. V. Photoinduced Electron Dynamics at the Chromophore—Semiconductor Interface: A Time-Domain Ab Initio Perspective. *Prog. Surf. Sci.* **2009,** *84*, 30–68.
(19) Kleiman, V. D.; Melinger, J. S.; McMorrow, D. Ultrafast Dynamics of Electronic Excitations in a Light-Harvesting Phenylacetylene Dendrimer. *J. Phys. Chem. B* **2001,** *105*, 5595–5598.
(20) Atas, E. Ultrafast Time Resolved Excitation Dynamics in Conjugated Dendrimers. *Chemistry*; University of Florida: Gainsville, FL, 2006.
(21) Kuroda, D. G.; et al. Mapping Excited-State Dynamics by Coherent Control of a Dendrimer's Photoemission Efficiency. *Science* **2009,** *326*, 263–267.
(22) Davydov, A. S. *Theory of Molecular Excitatios*; Plenum: New York, 1971.
(23) Rashba, E. I.; Sturge, M. D. *Excitons*; North Holland: Amsterdam, The Netherlands, 1982.
(24) Poliakov, E. Y.; et al. Exciton-Scaling and Optical Excitations of Self-Similar Phenylacetylene Dendrimers. *J. Chem. Phys.* **1999,** *110*, 8161–8175.
(25) Wong, C. Y. Ideal Dipole Approximation Fails to Predict Electronic Coupling and Energy Transfer between Semiconducting Single-Wall Carbon Nanotubes. *J. Chem. Phys.* **2009,** *130*, 081104.
(26) Beljonne, D.; et al. Beyond Förster Resonance Energy Transfer in Biological and Nanoscale Systems. *J. Phys. Chem. B* **2009,** *113*, 6583–6599.
(27) Thompson, A. L.; et al. Variable Electronic Coupling in Phenylacetylene Dendrimers: The Role of Forster, Dexter, And Charge-Transfer Interactions. *J. Phys. Chem. A* **2004,** *108*, 671–682.
(28) Devadoss, C.; Bharathi, P.; Moore, J. S. Energy Transfer in Dendritic Macromolecules: Molecular Size Effects and the Role of an Energy Gradient. *J. Am. Chem. Soc.* **1996,** *118*, 9635–9644.
(29) Xu, Z. F.; et al. Phenylacetylene Dendrimers by the Divergent, Convergent, and Double-Stage Convergent Methods. *J. Am. Chem. Soc.* **1994,** *116*, 4537–4550.
(30) Shortreed, M. R.; et al. Directed Energy Transfer Funnels in Dendrimeric Antenna Supermolecules. *J. Phys. Chem. B* **1997,** *101*, 6318–6322.
(31) Worth, G. A.; Robb, M. A.; Lasorne, B. Solving the Time-Dependent Schrodinger Equation for Nuclear Motion in One

Step: Direct Dynamics of Non-Adiabatic Systems. *Mol. Phys.* **2008,** *106*, 2077–2091.
(32) Hammes-Schiffer, S.; Tully, J. C. Proton Transfer in Solution: Molecular Dynamics with Quantum Transitions. *J. Chem. Phys.* **1994,** *101*, 4657–4667.
(33) Tully, J. C. Molecular Dynamics with Electronic Transitions. *J. Chem. Phys.* **1990,** *93*, 1061–1071.
(34) Tully, J. C. Nonadiabatic Molecular Dynamics. *Int. J. Quantum Chem.* **1991,** *40*, 299–309.
(35) Ben-Nun, M.; Quenneville, J.; Martinez, T. J. Ab Initio Multiple Spawning: Photochemistry from First Principles Quantum Molecular Dynamics. *J. Phys. Chem. A* **2000,** *104*, 5161–5175.
(36) Ben-Nun, M.; Martinez, T.J. Ab Initio Quantum Molecular Dynamics. *Adv. Chem. Phys.* **2002,** *121*, 439–512.
(37) Burghardt, I.; Meyer, H. D.; Cederbaum, L. S. Approaches to the Approximate Treatment of Complex Molecular Systems by the Multiconfiguration Time-Dependent Hartree Method. *J. Chem. Phys.* **1999,** *111*, 2927–2939.
(38) Lasorne, B.; Robb, M. A.; Worth, G. A. Direct Quantum Dynamics Using Variational Multi-Configuration Gaussian Wavepackets. Implementation Details and Test Case. *Phys. Chem. Chem. Phys.* **2007,** *9*, 3210–3227.
(39) Bearpark, M. J.; et al. The Azulene S_1 State Decays via a Conical Intersection: A CASSCF Study with MMVB Dynamics. *J. Am. Chem. Soc.* **1996,** *118*, 169–175.
(40) Bearpark, M. J.; et al. Can Fulvene S_1 Decay Be Controlled? A CASSCF Study with MMVB Dynamics. *J. Am. Chem. Soc.* **1996,** *118*, 5254–5260.
(41) Granucci, G.; Persico, M.; Toniolo, A. Direct Semiclassical Simulation of Photochemical Processes with Semiempirical Wave Functions. *J. Chem. Phys.* **2001,** *114*, 10608–10615.
(42) Bearpark, M. J.; et al. An Mc-Scf Study of Styrene Singlet-State Photoisomerization. *J. Am. Chem. Soc.* **1995,** *117*, 6944–6953.
(43) Markwick, P. R. L.; Doltsinis, N. L. Ultrafast Repair of Irradiated DNA: Nonadiabatic Ab Initio Simulations of the Guanine-Cytosine Photocycle. *J. Chem. Phys.* **2007,** *126*, 172102.
(44) Antol, I. Simulation of the Photodeactivation of Formamide in the n(O)−π^* and $\pi-\pi^*$ States: An Ab Initio on-the-Fly Surface-Hopping Dynamics Study. *J. Chem. Phys.* **2007,** *127*, 234303.
(45) Zechmann, G.; et al. Multiple Pathways in the Photodynamics of a Polar π-Bond: A Case Study of Silaethylene. *Chem. Phys. Lett.* **2006,** *418*, 377–382.
(46) Barbatti, M.; Aquino, A. J. A.; Lischka, H. A Multireference Configuration Interaction Investigation of the Excited-State Energy Surfaces of Fluoroethylene (C_2H_3F). *J. Phys. Chem. A* **2005,** *109*, 5168–5175.
(47) Barbatti, M.; et al. Semiempirical Molecular Dynamics Investigation of the Excited State Lifetime of Ethylene. *Chem. Phys. Lett.* **2005,** *401*, 276–281.
(48) Barbatti, M. The Nonadiabatic Deactivation Paths of Pyrrole. *J. Chem. Phys.* **2006,** *125*, 164323.
(49) Craig, C. F.; Duncan, W.R.; Prezhdo, O.V. Trajectory Surface Hopping in the Time-Dependent Kohn−Sham Approach for Electron-Nuclear Dynamics. *Phys. Rev. Lett.* **2005,** *95*, 163001.
(50) Worth, G. A.; Robb, M. A.; Burghardt, I. a Novel Algorithm for Non-Adiabatic Direct Dynamics Using Variational Gaussian Wavepackets. *Faraday Discuss.* **2004,** *127*, 307–323.
(51) Tretiak, S. Conformational Dynamics of Photoexcited Conjugated Molecules. *Phys. Rev. Lett.* **2002,** *89*, 097402.
(52) Tretiak, S. Photoexcited Breathers in Conjugated Polyenes: An Excited-State Molecular Dynamics Study. *Proc. Natl. Acad. Sci. U.S.A.* **2003,** *100*, 2185–2190.
(53) Fernandez-Alberti, S.; et al. Nonadiabatic Molecular Dynamics Simulations of the Energy Transfer between Building Blocks in a Phenylene Ethynylene Dendrimers. *J. Phys. Chem. A* **2009,** *113*, 7535–7542.
(54) Tretiak, S.; Chernyak, V.; Mukamel, S. Two-Dimensional Real-Space Analysis of Optical Excitations in Acceptor-Substituted Carotenoids. *J. Am. Chem. Soc.* **1997,** *119*, 11408–11419.
(55) Mukamel, S.; et al. Electonic Coherence and Collective Optical Excitations of Conjugated Molecules. *Science* **1997,** *277*, 781–787.
(56) Dewar, M. J. S.; et al. AM1: A New General Purpose Quantum Mechanical Molecular Model. *J. Am. Chem. Soc.* **1985,** *107*, 3902–3909.
(57) Franco, I.; Tretiak, S. Electron-Vibrational Relaxation of Photoexcited Polyfluorenes in the Presence of Chemical Defects: A Theoretical Study. *Chem. Phys. Lett.* **2003,** *372*, 403–408.
(58) Franco, I.; Tretiak, S. Electron-Vibrational Dynamics of Photoexcited Polyfluorenes. *J. Am. Chem. Soc.* **2004,** *126*, 12130–12140.
(59) Tretiak, S.; et al. CEO/Semiempirical Calculations of UV−Visible Spectra in Conjugated Molecules. *Chem. Phys. Lett.* **2000,** *331*, 561–568.
(60) Collini, E.; Scholes, G. D. Coherent Intrachain Energy Migration in a Conjugated Polymer at Room Temperature. *Science* **2009,** *323*, 369–373.
(61) Paterlini, M. G.; Ferguson, D. M. Constant Temperature Simulations Using the Langevin Equation with Velocity Verlet Integration. *Chem. Phys.* **1998,** *236*, 243–252.
(62) Curutchet, C.; et al. Electronic Energy Transfer in Condensed Phase Studied by a Polarizable QM/MM Model. *J. Chem. Theory Comput.* **2009,** *5*, 1838–1848.
(63) Verlet, L. Computer Experiments on Classical Fluids. I. Thermodynamical Properties of Lennard-Jones Molecules. *Phys. Rev.* **1967,** *159*, 98.
(64) Allen, M. P.; Tildesley, D. J. *Computer Simulation of Liquids*; Clarendon Press: Oxford, U.K., 1987.
(65) Tommasini, M.; Chernyak, V.; Mukamel, S. Electronic Density-Matrix Algorithm for Nonadiabatic Couplings in Molecular Dynamics Simulations. *Int. J. Quantum Chem.* **2001,** *85*, 225–238.
(66) Scholes, G. D.; Rumbles, G. Excitons in Nanoscale Systems. *Nat. Mater.* **2006,** *5*, 683–696.

DOI: 10.1021/jz100794z | *J. Phys. Chem. Lett.* **2010,** *1*, 2699–2704